How Will Orographic Precipitation Respond to Surface Warming?–An Idealized Thermodynamic Perspective

Nicholas Siler,[1] Gerard Roe,[2]

Future changes in orographic precipitation will have important consequences for societies and ecosystems near mountain ranges. Here we use a simple numerical model to evaluate the response of orographic precipitation to surface warming under idealized conditions representative of the strongest orographic storms. We find an upward shift in the pattern of condensation with warming, caused by larger fractional changes in condensation at low temperature and amplified warming aloft. As a result, the distribution of precipitation shifts downwind, causing larger fractional changes in precipitation on the lee slope than on the windward slope. Total precipitation is found to increase by a smaller fraction than near-surface water vapor, in contrast to expected changes in other types of extreme precipitation. Factors limiting the increase in orographic precipitation include the pattern of windward ascent, lee-side evaporation, and thermodynamic constraints on the change in condensation with temperature.

1. Introduction

Significant changes are expected in the amount, frequency, and distribution of precipitation as the climate warms. Nowhere are the consequences of such changes likely to be greater than in mountains, which supply half the world's population with fresh water [*Beniston*, 2005], and which are often particularly susceptible to flooding from intense precipitation [e.g., *Bougeault et al.*, 2001].

The way that orographic precipitation will respond to climate change depends on a variety of factors. In some mountain ranges, a higher freezing level may cause a shift from snow to rain, resulting in less snowpack and higher flood risk [e.g., *Leung et al.*, 2004]. In addition, large-scale shifts in wind speed or direction may alter atmospheric moisture transport or mountain-wave dynamics, affecting where and how much precipitation falls [e.g., *Shi and Durran*, 2013; *Siler et al.*, 2013]. To account for these and myriad other factors, sophisticated regional climate models (RCMs) have been used to simulate the response to greenhouse forcing in mountainous regions of Europe and western North America, where global climate models do not adequately resolve the terrain [e.g., *Hewitt*, 2004; *Mearns et al.*, 2009]. But while RCMs provide great detail, their complexity can inhibit physical understanding.

Here we take a simpler approach, highlighting one robust aspect of the response of orographic precipitation to surface warming. Under idealized conditions that pertain to many strong midlatitude storms, we consider how changes in the pattern of upslope condensation may alter the amount and distribution of orographic precipitation. Our reasons for this approach are two-fold. First, while the total change in orographic precipitation may be complex and mountain-range specific, the thermodynamic laws governing condensation are well understood and universally applicable. Second, although the change in condensation with warming has been discussed in previous studies of extreme precipitation [e.g., *Trenberth*, 1999; *O'Gorman and Schneider*, 2009] and orographic drying ratios [*Kirshbaum and Smith*, 2008], its application to orographic precipitation has not specifically been addressed.

While there are many different types of orographic precipitation [e.g., *Houze*, 2012], here we focus on the classic two-dimensional picture, which is most applicable to mid-latitude ranges like the Cascades and the Sierra Nevada whose axes lie perpendicular to the prevailing westerly winds. In these ranges, moist air flowing off the Pacific rises as it encounters the topography, enhancing condensation over the western slope. Some of this condensate eventually becomes rain or snow, which falls toward the surface while also being advected downwind. East of the crest, descending air warms and desiccates, causing what condensate remains in the air to evaporate.

With this picture in mind, we ask the following question: for a given storm, how will a rise in sea-level temperature (T_s) alter the amount and distribution of precipitation across a mountain range? We present results for an idealized storm in which the troposphere upstream of the ridge is both saturated and moist-adiabatic (i.e., pseudoequivalent potential temperature is constant with height) [*Emanuel*, 1994]. These conditions, while not representative of orographic storms in general, are a reasonable approximation of "atmospheric rivers" (ARs) [e.g., *Ralph et al.*, 2005], which are long bands of moist, tropical air flowing poleward and eastward within the warm sectors of mid-latitude cyclones [*Newell et al.*, 1992]. ARs are responsible for up to half the total annual precipitation–and virtually all major floods–in mid-latitude coastal ranges like the Cascades and the Sierra Nevada, and are therefore a natural starting point for understanding the overall impact of climate change on mid-latitude orographic precipitation [*Guan et al.*, 2010; *Neiman et al.*, 2011; *Dettinger et al.*, 2011].

2. Model Description and Results

Our analysis consists of simulations of moist flow over a two-dimensional ridge of the form

$$h(x) = h_0 e^{-(x/\sigma)^2}, \tag{1}$$

with $h_0 = 1$ km and $\sigma = 25$ km, chosen as a rough approximation of the Cascades. Our model applies a warm-rain microphysical parameterization to dynamical fields derived from linear mountain-wave theory (see Appendix A for details). Simulations are performed at sea-level temperatures of 13°C and 15°C, with the former representing a typical

[1]Department of Atmospheric Sciences, University of Washington, Seattle, WA, USA.
[2]Department of Earth and Space Sciences, University of Washington, Seattle, WA, USA.

0094-8276/14/$5.00

AR in today's climate, and the latter representing estimated warming by the end of the century [*Dettinger*, 2011]. Within ascending regions upstream of the ridge, the troposphere is assumed to be saturated and moist-adiabatic, with a sea-level pressure of 1000 hPa in both simulations. Under these conditions, the condensation rate in ascending regions upstream of the ridge is given by

$$C = -\nabla \cdot (\mathbf{u}\rho q) \simeq -w\rho\frac{dq}{dz}, \tag{2}$$

where $\mathbf{u}$ is the two-dimensional wind vector, $w(x,z)$ is the vertical wind speed, $\rho(z)$ is the air density, and $q(z)$ is the specific humidity. In the lee, temperature and humidity are controlled by adiabatic descent and evaporation. The background flow is assumed to be perpendicular to the ridge axis, with a uniform speed of 23 m/s based on observations of ARs over the Pacific Ocean [*Ralph et al.*, 2005]. The model is initiated without liquid water and integrated forward in time until steady-state is reached ($\sim$ 2 hrs).

We begin by examining how the pattern of upslope condensation changes in response to surface warming. Figure 1a shows C (shaded contours) and w (solid contours) in the control simulation (i.e., $T_s = 13^\circ$C). Figure 1b shows the difference in condensation (δC) between the two simulations, along with example hydrometeor trajectories in each simulation. In contrast to C, which is concentrated near the surface, δC increases with height in the lower troposphere, reaching a maximum value between 2 and 3 km.

To understand why the patterns of C and δC are so different, it is helpful to approximate δC as the product of three different terms,

$$\delta C \approx C \cdot \delta T \cdot \frac{d\ln C}{dT}, \tag{3}$$

where $\delta T(z)$ is the difference in temperature between the two simulations. From this equation, it is clear that δT and $d\ln C/dT$ must collectively be acting to shift the pattern of δC upward relative to C.

Let us consider the contribution from each of these terms independently. The first term, δT, increases with height as a result of the "lapse-rate effect", or the decrease in moist-adiabatic lapse rate with temperature [e.g., *Emanuel*, 1994]. Thus, while T_s differs by only 2°C between the two simulations, the temperature at 6 km differs by more than 4°C. From Equation 3, this contributes to an amplification of δC aloft.

The other term, $d\ln C/dT$, represents the fractional change in condensation with temperature. Given fixed w, this term behaves much like the saturation vapor pressure, which scales as T^{-2} in the Clausius-Clapeyron equation (see Appendix B). Since temperature decreases with height, this implies a larger fractional change in condensation at high altitudes.

The relative importance of these two factors is illustrated in Figure 1c. The black line represents the total fractional change in condensation as a function of altitude, which ranges from 4% at the surface to more than 50% in the upper troposphere. The blue line shows what the fractional change would be if warming were uniform throughout the column. The difference between the black and blue lines is shown in red, and can be interpreted as the contribution from the lapse-rate effect. While the lapse-rate contribution is minimal in the lower troposphere, it accounts for most of the increase in condensation above 6km.

How does the pattern of δC in Figure 1b impact precipitation at the surface? Figure 2 shows the precipitation rate P in the two simulations along with the fractional change in precipitation with warming ($\delta P/P$). Clear differences are evident in the shapes of the two curves: while P is concentrated over the windward slope, $\delta P/P$ is highest in the lee, indicative of a downwind shift in the precipitation distribution.

We can understand this shift in precipitation by considering the hydrometeor trajectories in Figure 1b. The trajectories were calculated using the mass-weighted average fall speed of all hydrometeors in each grid cell, and therefore provide a rough indication of where surface precipitation originates. The trajectories reveal two competing factors influencing the pattern of precipitation change. First, the trajectories in the warmer simulation (dashed lines) are steeper than those in the control simulation (solid lines), indicative of a faster hydrometeor fall speed. This difference reflects a larger rain-water mixing ratio in the warmer case as a direct consequence of enhanced condensation. By itself, the increase in hydrometeor fall speeds with warming would favor an *upwind* shift in the precipitation distribution.

That precipitation instead shifts *downwind* is the result of a second, more important influence, which relates to the different altitudes at which condensation is sampled across the ridge. At low elevations upwind of the crest, the precipitation that reaches the surface originates low in the atmosphere, where the fractional change in condensation is minimal. Further downwind, precipitation originates at increasingly higher altitudes where condensation is more sensitive to warming, resulting in larger values of $\delta P/P$. If hydrometeor fall speeds were the same in both simulations, the increase in $\delta P/P$ with distance downwind would be even more pronounced, as indicated by the grey dashed line in Figure 2.

Interestingly, $\delta P/P$ does not increase monotonically with distance downwind, but declines beyond about 10 km downwind of the crest. This behavior is partially caused by the difference in hydrometeor fall speeds discussed above. However, similar behavior is evident even when hydrometeor fall speeds are held constant (grey dashed line, Figure 2), implying that the warmer simulation must also exhibit greater evaporation in the lee. Since $d\theta/dz$ increases with temperature under moist-adiabatic conditions, an increase in surface temperature implies greater adiabatic warming with lee-side descent, resulting in lower relative humidities and enhanced evaporation. In the far lee, the increase in evaporation in the warmer simulation more than compensates for the increase in condensation upstream, resulting in less precipitation (i.e. negative $\delta P/P$). However, this occurs only where precipitation is quite low to begin with, and its impact on total precipitation is therefore minimal.

Overall, precipitation is 9.3% greater in the warmer simulation than in the control simulation. Upstream of the crest, the increase is 8.8%; in the lee, it is 12.2%. By comparison, precipitation from strong non-orographic storms is generally thought to scale with near-surface water vapor [e.g., *Trenberth*, 1999; *O'Gorman and Schneider*, 2009; *Muller et al.*, 2011], which increases by 13.1% in our simulations. This suggests that in the absence of dynamical changes, orographic precipitation is likely to increase at a lower rate than intense precipitation in non-mountainous regions.

There are two reasons for the relatively muted response of precipitation to surface warming within our model. The first and most important reason is that the increase in upstream condensation is itself quite modest, at 11.8%. This change is much smaller than the 19.7% increase in tropospheric water vapor, implying that a smaller fraction of the cross-ridge moisture flux is condensed in the warmer simulation. Some of this difference is due to the fact that $d\ln C/dT$ is smaller than the fractional change in water vapor, which has been noted previously [*O'Gorman and Schneider*, 2009;

Kirshbaum and Smith, 2008], and is discussed further in Appendix B. An additional factor constraining the increase in condensation within our simulations is the pattern of windward ascent, which is largest near the surface and decreases with height (Figure 1a). This gives more weighting to the lower atmosphere, where for the reasons discussed above, the sensitivity of condensation to warming is comparatively small.

A further constraint on the increase in precipitation with surface warming is the vertical distribution of condensation change (Figure 1b). Because much of the condensation change occurs aloft, some of the additional condensate in the warmer simulation evaporates in the lee before reaching the surface. This explains why the increase in total precipitation, at 9.3%, is less than the 11.8% increase in upstream condensation.

To test the sensitivity of our results to the dimensions of the ridge, we performed a series of additional simulations using ridges of the same general shape (Equation 1), but with h_0 ranging from 500 to 1500 meters, and with σ ranging from 10 to 40 km. Here we consider only the fractional change in precipitation as the sea-level temperature is raised from 13°C to 15°C.

All else being equal, the taller and wider the ridge, the larger the fractional change in precipitation on both sides of the crest (Table 1). Since the change in condensation is similar in all simulations, this implies that the height and width of a ridge affect how much of the additional condensate reaches the surface as precipitation. Taller ridges are more effective at intercepting rain drops as they are advected downwind, while wider ridges allow more time for rain drops to reach the surface before evaporating in the lee. In both cases, more condensate is extracted from high in the atmosphere where sensitivity to warming is greatest, resulting in larger fractional changes in precipitation.

While ridge size has a modest effect on the total change in precipitation with warming, larger increases in the lee are evident in all cases, reflecting a consistent downwind shift in the distribution of precipitation. In addition, the increase in total precipitation is less than 10% even for the tallest and widest ridge–still much smaller than the increase in both upstream condensation and moisture flux.

An additional sensitivity test was performed using the original ridge dimensions but with $U = 15$ and 30 m/s, which spans the typical range of observed conditions during Pacific ARs [*Ralph et al.*, 2005]. A priori, one might expect that increasing (decreasing) U would have much the same effect as decreasing (increasing) σ, since their ratio sets the timescale for cross-ridge advection. However, we instead find that U has little impact on the change in precipitation with warming. When $U = 15$ m/s, the change in total precipitation with warming is 9.7%; when $U = 30$ m/s, it is 9.4%. The reason for this insensitivity is microphysical: a stronger U results in enhanced condensation rates, faster hydrometeor fall speeds, and more efficient accretion of cloud water, while a weaker U has the opposite effect. These microphysical changes largely offset the more obvious impact of U on cross-ridge advection.

3. Discussion

In this paper, we have used a simple model to evaluate the change in orographic precipitation with surface warming assuming fixed storm dynamics. Under idealized conditions typical of atmospheric rivers, we found that surface warming induces an upward shift in the pattern of windward condensation, which in turn causes a downwind shift in the distribution of precipitation. As a result, the fractional change in precipitation is larger on the lee slope than on the windward slope. We also found that the increase in total precipitation is limited by a number of factors, including the pattern of windward ascent, lee-side evaporation, and thermodynamic constraints on $d \ln C/dT$. Thus, for 2°C of surface warming, the increase in total precipitation is just 9.3%. By comparison, intense non-orographic precipitation is thought to scale roughly with near-surface water vapor, which increases by 13.1% in our simulations.

Even though these results are specific to storms with saturated, moist-adiabatic conditions, they may have relevance for other types of orographic storms as well. In particular, an upward shift in the pattern of condensation with warming will apply to any storm in which the magnitude of warming and the fractional change in condensation increase with height, suggesting that the downwind shift in precipitation observed here is likely to be robust. Additionally, in storms with higher static stabilities, windward ascent tends to be concentrated closer to the surface [e.g., *Smith*, 1979], which would suggest an even smaller fractional change in precipitation than observed here.

It is important to emphasize that factors besides those considered here may also affect how orographic precipitation responds to climate change. For example, an increase in freezing level is likely to increase the ratio of liquid to solid hydrometeors. Given the faster average fall speeds of liquid hydrometeors, this change would likely tend to shift the distribution of precipitation upwind, perhaps counteracting the thermodynamic response discussed here [*Pavelsky et al.*, 2012]. In addition, changes in the location or dynamics of mid-latitude storms could turn out to be more important than thermodynamic changes in certain mountain ranges, as *Shi and Durran* [2013] have demonstrated within an idealized aquaplanet GCM.

Nevertheless, there is some evidence that the thermodynamic changes identified in this paper may be of primary importance, at least within the Cascades and the Sierra Nevada. In the Sierra Nevada, for example, unusually warm atmospheric rivers have been shown to cause flooding disproportionately in lee-side watersheds, as our simulations would predict [*Underwood et al.*, 2009]. In addition, at least two ensembles of regional climate change simulations over western North America give predictions that appear to be consistent with our results, with the largest fractional changes in both mean and extreme wintertime precipitation occurring in the immediate lee of the Cascades and the Sierra Nevada, and relatively modest increases on windward slopes [*Diffenbaugh et al.*, 2005; *Wehner*, 2013]. While much more research is needed to understand the full response of orographic precipitation to climate change in any particular mountain range, we hope that our results might serve as a useful benchmark against which other predictions can be interpreted and evaluated.

Appendix A: Model details

A1. Dynamics

Dynamical fields within our model are derived from the linear, inviscid, hydrostatic, Boussinesq equations of motion within a stably stratified atmosphere in steady-state. Given a constant background wind speed U, w is governed by

$$\frac{d^2w}{dz^2} + \frac{N^2}{U^2}w = 0, \tag{A1}$$

where $N(z)$ is the Brunt-Väisälä frequency.

We solve for w within a two-layer atmosphere, with a tropopause height $H = 10$ km. In the stratosphere, we

set $N = 0.02$ s^{-1}. In the troposphere, we follow a common convention [e.g., *Smith and Barstad*, 2004; *Kunz and Kottmeier*, 2006], and use the moist Brunt-Väisälä frequency, N_m, which under moist-adiabatic conditions is given by

$$N_m^2 = -\frac{g}{1+r}\frac{dr}{dz}, \tag{A2}$$

where g is the acceleration of gravity and r is the total water mixing ratio [*Durran and Klemp*, 1982]. Neglecting the contribution from liquid water, we find that to good approximation,

$$N_m^2 \approx N_0^2\left(1 - \frac{z}{H}\right), \tag{A3}$$

with $N_0^2 = 2\times10^{-5}$ s^{-1}. For the sea-level temperatures we simulate, this approximation implies a vertical temperature profile that differs from the moist-adiabatic profile by less than 0.3K throughout the column.

Using this approximation, the solution to (A1) within the troposphere is found to be

$$\begin{aligned} w(x,z) &= \alpha(x)Ai\left[\left(\frac{N_0}{HU}\right)^{2/3}(z-H)\right] \\ &\quad +\beta(x)Bi\left[\left(\frac{N_0}{HU}\right)^{2/3}(z-H)\right]. \end{aligned} \tag{A4}$$

Here Ai and Bi represent Airy functions of the first and second kind, while $\alpha(x)$ and $\beta(x)$ are found by applying the conventional boundary and matching conditions [e.g., *Klemp and Lilly*, 1975]. The perturbation horizontal wind, u, is determined via (A4) and the continuity equation.

One potential problem with using linear dynamical fields is that the lower boundary condition is applied at $z = 0$ rather than at the terrain height, which can result in spurious flow into or out of the surface. However, for the flow field described by (A4) with $U = 23$ m/s, an air parcel that starts at sea level upstream of the ridge follows the terrain to within five meters across the entire domain, demonstrating that the linear solution satisfies the actual lower boundary condition very well.

A2. Microphysics

We use a bulk warm-rain microphysical parameterization based on that of *Kessler* [1969], but with three differences. First, Kessler assumed that the terminal velocity V of a rain drop is proportional to the square root of the drop diameter D. We instead use an empirical formula derived by *Liu and Orville* [1969], which gives $V \propto D^{4/5}$. The greater dependence on D causes larger changes in hydrometeor trajectories with warming (Figure 1b). Second, our treatment of rain-water evaporation follows *Gregory* [1995], and produces somewhat slower evaporation than Kessler's scheme, allowing more rain to reach lee slopes. Third, autoconversion in the Kessler scheme is represented as

$$\frac{Dl_r}{Dt} = \tau(l_c - l_0), \tag{A5}$$

where l_r and l_c are the mixing ratios of rain and cloud water, l_0 is a precipitation threshold for cloud water (often set to 10^{-3} g g^{-1}) and τ is a positive rate constant (equal to 0 when $l_c < l_0$, and often set to 10^{-3} s^{-1} otherwise). In this treatment, precipitation is not initiated until the precipitation threshold is exceeded. While this is reasonable in many cases, it does not make sense in our simulations because intense orographic precipitation is nearly always accompanied by large-scale precipitation, which significantly reduces the residence time of cloud water [e.g., *Cotton et al.*, 2010], and which renders the precipitation threshold moot. To account for this effect in our model, therefore, we set $C = 10^{-2}$ s^{-1} and $l_0 = 0$. While somewhat arbitrary, we believe that these values are a reasonable representation of what actually occurs during intense orographic storms.

Appendix B: Decomposition of $d\ln C/dT$

Using the hydrostatic approximation,

$$\frac{dp}{dz} = -\rho g, \tag{B1}$$

and the following relations,

$$q \equiv \frac{\epsilon e_s}{p - (1-\epsilon)e_s} \tag{B2}$$

$$\rho = \frac{p - (1-\epsilon)e_s}{R_d T}, \tag{B3}$$

Equation 2 can be rewritten as

$$C = w\frac{e_s\beta}{R_v^2 T^2}, \tag{B4}$$

where

$$\beta \equiv \frac{L_v\Gamma_m}{T}\left(\frac{p}{p-(1-\epsilon)e_s}\right) + \frac{g}{\epsilon}. \tag{B5}$$

Here e_s is the saturation vapor pressure, T is temperature, L_v is the latent heat of vaporization, Γ_m is the moist-adiabatic lapse rate (dT/dz), p is pressure, g is the acceleration due to gravity, R_d and R_v are the specific gas constants of dry air and water vapor, $\epsilon = R_d/R_v$, and w, ρ, and q are defined in Equation 2. Therefore, given fixed dynamics,

$$\frac{d\ln C}{dT} = \frac{d\ln e_s}{dT} + \frac{d\ln\beta}{dT} - \frac{2}{T}. \tag{B6}$$

Of the three terms on the RHS of (B6), the first is the largest in magnitude and contributes most to the increase in $d\ln C/dT$ with height. Its value is given by the Clausius-Clapeyron equation,

$$\frac{d\ln e_s}{dT} = \frac{L_v}{R_v T^2}, \tag{B7}$$

and ranges from just over 6%/K at the surface to 13%/K at the tropopause within our simulations. By comparison, the second term, influenced primarily by the temperature-dependence of Γ_m, ranges from about -4%/K at the surface to -1%/K at the tropopause, while the third term is also negative but generally smaller in magnitude (< 1%/K).

Two conclusions can be drawn from this analysis. First, the increase in $d\ln C/dT$ with height is primarily due to the increase in $d\ln e_s/dT$ at colder temperatures. Second, $d\ln C/dT$ is smaller than $d\ln e_s/dT$ because of the second and third terms in (B6), which partially explains why the increase in condensation is less than the increase in atmospheric water vapor within our simulations.

Acknowledgments. This work was supported by the National Defense Science and Engineering Graduate Fellowship and by National Science Foundation Grant AGS-1138977.

References

Beniston, M. (2005), Mountain climates and climatic change: an overview of processes focusing on the European Alps, *Pure Appl. Geophys.*, *162*(8-9), 1587–1606, doi:10.1007/s00024-005-2684-9.

Bougeault, P., P. Binder, A. Buzzi, R. Dirks, J. Kuettner, R. Houze, R. B. Smith, R. Steinacker, and H. Volkert (2001), The MAP special observing period, *Bull. Amer. Meteor. Soc.*, *82*(3), 433–462, doi:10.1175/1520-0477(2001)082<0433:TMSOP>2.3.CO;2.

Cotton, W. R., G. Bryan, and S. C. van den Heever (2010), *Storm and cloud dynamics*, 820 pp., Academic Press, San Diego.

Dettinger, M. (2011), Climate change, atmospheric rivers, and floods in California - a multimodel analysis of storm frequency and magnitude changes, *J. Am. Water Resour. Assoc.*, *47*(3), 514–523, doi:10.1111/j.1752-1688.2011.00546.x.

Dettinger, M. D., F. M. Ralph, T. Das, P. J. Neiman, and D. R. Cayan (2011), Atmospheric rivers, floods and the water resources of california, *Water*, *3*(4), 445–478, doi:10.3390/w3020445.

Diffenbaugh, N. S., J. S. Pal, R. J. Trapp, and F. Giorgi (2005), Fine-scale processes regulate the response of extreme events to global climate change, *Proc. Natl. Acad. Sci. U. S. A.*, *102*(44), 15,774–8, doi:10.1073/pnas.0506042102.

Durran, D. R., and J. B. Klemp (1982), On the effects of moisture on the Brunt-Väisälä frequency, *J. Atmos. Sci.*, *39*(10), 2152–2158, doi:10.1175/1520-0469(1982)039<2152:OTEOMO>2.0.CO;2.

Emanuel, K. (1994), *Atmospheric convection*, 580 pp., Oxford Univ. Press, New York.

Gregory, D. (1995), A consistent treatment of the evaporation of rain and snow for use in large-scale models, *Mon. Wea. Rev.*, *123*(9), 2716–2732, doi:10.1175/1520-0493(1995)123<2716:ACTOTE>2.0.CO;2.

Guan, B., N. P. Molotch, D. E. Waliser, E. J. Fetzer, and P. J. Neiman (2010), Extreme snowfall events linked to atmospheric rivers and surface air temperature via satellite measurements, *Geophys. Res. Lett.*, *37*(L20401), doi:10.1029/2010GL044696.

Hewitt, C. D. (2004), Ensembles-based predictions of climate changes and their impacts, *Eos, Trans., Am. Geophys. Union*, *85*(52), 566, doi:10.1029/2004EO520005.

Houze, R. A. (2012), Orographic effects on precipitating clouds, *Rev. Geophys.*, *50*(1), RG1001, doi:10.1029/2011RG000365.

Kessler, E. (1969), On the distribution and continuity of water substance in atmospheric circulation, *Meteor. Monogr.*, *10*.

Kirshbaum, D. J., and R. B. Smith (2008), Temperature and moist-stability effects on midlatitude orographic precipitation, *Quart. J. Roy. Meteor. Soc.*, *134*(634), 1183–1199, doi:10.1002/qj.274.

Klemp, J. B., and D. R. Lilly (1975), The dynamics of wave-induced downslope winds, *J. Atmos. Sci.*, *32*(2), 320–339, doi:10.1175/1520-0469(1975)032<0320:TDOWID>2.0.CO;2.

Kunz, M., and C. Kottmeier (2006), Orographic enhancement of precipitation over low mountain ranges. Part I: model formulation and idealized simulations, *J. Appl. Meteor. Climatol.*, *45*(8), 1025–1040, doi:10.1175/JAM2389.1.

Leung, L. R., Y. Qian, X. Bian, W. M. Washington, J. Han, and J. O. Roads (2004), Mid-century ensemble regional climate change scenarios for the western United States, *Climatic Change*, *62*(1-3), 75–113, doi:10.1023/B:CLIM.0000013692.50640.55.

Liu, J. Y., and H. D. Orville (1969), Numerical modeling of precipitation and cloud shadow effects on mountain-induced cumuli, *J. Atmos. Sci.*, *26*(6), 1283–1298, doi:10.1175/1520-0469(1969)026<1283:NMOPAC>2.0.CO;2.

Mearns, L. O., W. Gutowski, R. Jones, R. Leung, S. McGinnis, A. Nunes, and Y. Qian (2009), A regional climate change assessment program for North America, *Eos, Trans., Am. Geophys. Union*, *90*(36), 311–311, doi:10.1029/2009EO360002.

Muller, C. J., P. a. OGorman, and L. E. Back (2011), Intensification of precipitation extremes with warming in a cloud-resolving model, *J. Climate*, *24*(11), 2784–2800, doi:10.1175/2011JCLI3876.1.

Neiman, P. J., L. J. Schick, F. M. Ralph, M. Hughes, and G. a. Wick (2011), Flooding in western Washington: the connection to atmospheric rivers, *J. Hydrometeor.*, *12*(6), 1337–1358, doi:10.1175/2011JHM1358.1.

Newell, R. E., N. E. Newell, Y. Zhu, and C. Scott (1992), Tropospheric rivers?–A pilot study, *Geophys. Res. Lett.*, *19*(24), 2401–2404.

O'Gorman, P. A., and T. Schneider (2009), The physical basis for increases in precipitation extremes in simulations of 21st-century climate change, *Proc. Natl. Acad. Sci. U. S. A.*, *106*(35), 14,773–7, doi:10.1073/pnas.0907610106.

Pavelsky, T. M., S. Sobolowski, S. B. Kapnick, and J. B. Barnes (2012) Changes in orographic precipitation patterns caused by a shift from snow to rain, *Geophys. Res. Lett.*, *39*(L18706), doi:10.1029/2012GL052741.

Ralph, F. M., P. J. Neiman, and R. Rotunno (2005), Dropsonde observations in low-Level jets over the northeastern Pacific Ocean from CALJET-1998 and PACJET-2001: mean vertical profile and atmospheric-river characteristics, *Mon. Wea. Rev.*, *133*(4), 889–910, doi:10.1175/MWR2896.1.

Shi, X., and D. R. Durran (2013), The response of orographic precipitation over idealized mid-latitude mountains due to global increases in CO2, *J. Climate*, doi:10.1175/JCLI-D-13-00460.1, In press.

Siler, N., G. Roe, and D. Durran (2013), On the dynamical causes of variability in the rain-shadow effect: a case study of the Washington Cascades, *J. Hydrometeor.*, *14*(1), 122–139, doi:10.1175/JHM-D-12-045.1.

Smith, R. B. (1979), The influence of mountains on the atmosphere, in *Adv. Geophys., Vol. 21*, pp. 87–230.

Smith, R. B., and I. Barstad (2004), A linear theory of orographic precipitation, *J. Atmos. Sci.*, *61*(12), 1377–1391, doi:10.1175/1520-0469(2004)061<1377:ALTOOP>2.0.CO;2.

Trenberth, K. (1999), Conceptual framework for changes of extremes of the hydrological cycle with climate change, *Climatic Change*, *42*(1), 327–339, doi:10.1023/a:1005488920935.

Underwood, S. J., M. L. Kaplan, and K. C. King (2009), The role of upstream midtropospheric circulations in the Sierra Nevada enabling leeside (spillover) precipitation. Part I: a synoptic-scale analysis of spillover precipitation and flooding in a leeside basin, *J. Hydrometeor.*, *10*(6), 1309–1326, doi:10.1175/2009JHM1105.1.

Wehner, M. F. (2013), Very extreme seasonal precipitation in the NARCCAP ensemble: model performance and projections, *Climate Dynamics*, *40*(1-2), 59–80, doi:10.1007/s00382-012-1393-1.

Corresponding author: N. T. Siler, Department of Atmospheric Sciences, University of Washington, Box 351640, Seattle, WA 98195, USA. (siler@uw.edu)

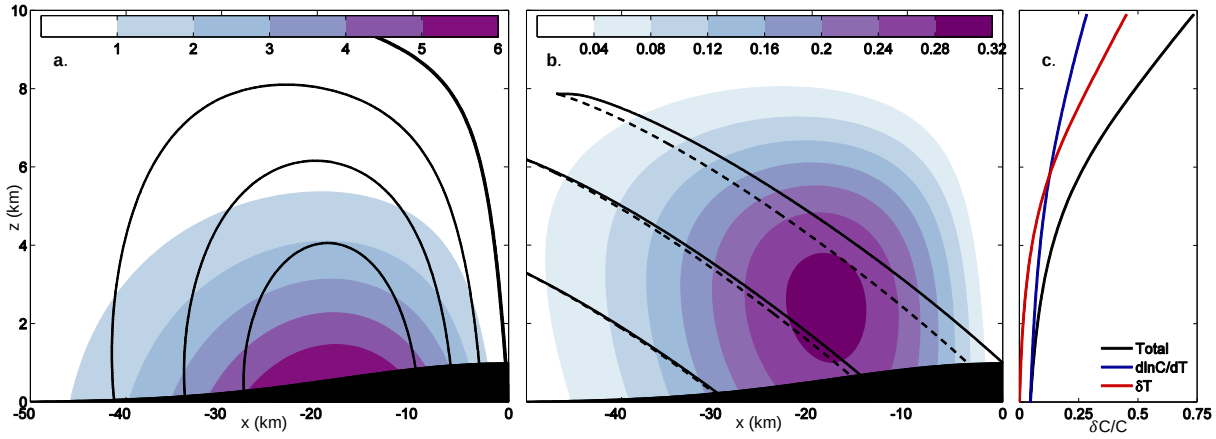

Figure 1. a) Condensation rate (colored shading; g m^{-3} hr^{-1}) and vertical velocity (solid contours; 0.2 m/s intervals) in the control simulation (T_s = 13°C). The thick solid contour represents $w = 0$. b) The difference in condensation rate between the warmed and control simulations (colored shading), and examples of bulk hydrometeor trajectories in the control (solid lines) and warmed (dashed lines) simulations. c) Black line: the fractional change in condensation as a function of altitude ($\delta C/C$); Blue line: $\delta C/C$ if warming were uniform throughout the column; Red line: the contribution to $\delta C/C$ from the lapse-rate effect (i.e., the amplification of warming aloft).

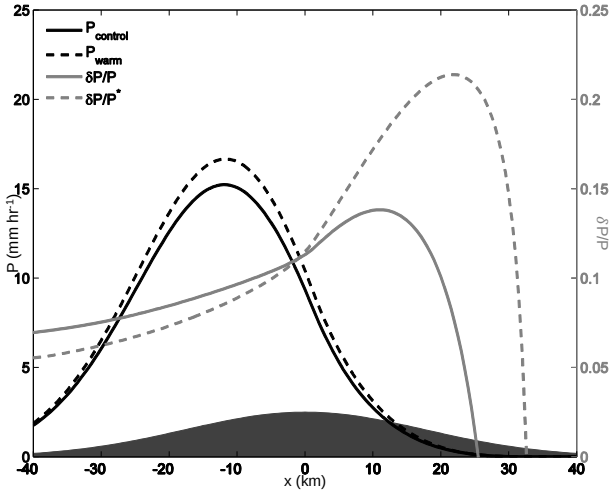

Figure 2. Black lines, left $y-$axis: precipitation rate in the control (solid line) and warmed (dashed line) simulations; Grey lines, right $y-$axis: the fractional change in precipitation ($\delta P/P$, solid line), and what $\delta P/P$ would be if hydrometeor trajectories were unchanged with warming ($\delta P/P^*$, dashed line).

Table 1. The percent change in windward, leeward, and total precipitation for various ridge sizes.[a]

Ridge	Windward	Leeward	Total
$\sigma = 10$ km			
$h_0 = 0.5$ km	6.7	9.3	8.0
$h_0 = 1$ km	8.3	11.2	8.8
$h_0 = 1.5$ km	8.8	11.4	9.1
$\sigma = 25$ km			
$h_0 = 0.5$ km	7.3	10.8	8.7
$h_0 = 1$ km	8.8	12.2	9.3
$h_0 = 1.5$ km	9.3	12.3	9.5
$\sigma = 40$ km			
$h_0 = 0.5$ km	7.9	11.7	9.2
$h_0 = 1$ km	9.3	13.1	9.8
$h_0 = 1.5$ km	9.7	13.3	9.9

[a] Values represent the difference in precipitation between the warm simulation ($T_s = 15°$C) and the control simulation ($T_s = 13°$C), divided by precipitation in the control simulation, multiplied by 100. Windward (leeward) precipitation is the total precipitation upwind (downwind) of the ridge crest.